A COMPARATIVE STUDY OF ISOTOPIC DEPENDENCE OF FUSION DYNAMICS FOR Ca–Ni COLLIDING SERIES

Narinder K. Dhiman, Rajeev K. Puri[†]

Department of Physics, Panjab University
Chandigarh-160 014, India

(Received November 21, 2005; revised version received January 9, 2006)

The fusion dynamics is studied in heavy-ion collisions over wide range of neutron content ($0.5 \leq N/Z \leq 2.0$) by employing several different theoretical models such as Skyrme energy density model and proximity potential, as well as parameterized potentials due to Bass, Christensen and Winther, Ngô and Ngô and Denisov. We find that all these potentials give similar isotopic dependence for the fusion barrier heights, positions as well as cross-sections. Fusion barrier heights and positions follow a second order non-linear isotopic dependence whereas fusion cross-sections follow a linear dependence. The collision of neutron-deficient nuclei results into a reduced fusion cross-section whereas collision of neutron-rich nuclei leads to an enhanced fusion probability. The maximal isotopic dependence is obtained for the near barrier energies that reduces to insignificant level for higher incident energies. Our normalised observations are almost model independent indicating the universality in these predictions.

PACS numbers: 24.10.–i, 25.70.Jj, 25.60.Pj, 25.70.–z

1. Introduction

It is now well accepted that the nuclear potential is the key factor in deciding the fate of a colliding pair of any size. Depending on the incident energy and (geometrical) impact parameter, the dominance of the nuclear potential can be judged [1]. When the colliding nuclei are mildly excited (for example, when either incident energy of the projectile is very low or impact parameter is very large) the nuclear potential (*i.e.* the real part of the G-matrix) plays a dominant role [1]. On the other hand, when either the incident energy is very high or impact parameter is very small, the violent nature of the reaction pushes the nuclear potential to insignificant level. In

[†] Corresponding author e-mail: `rkpuri@pu.ac.in`

this situation, the sub-atomic degrees of freedom start appearing and several new phenomena (like the multifragmentation, nuclear flow, stopping as well as sub-threshold particle production *etc.*) start dominating the reaction dynamics [1]. Since, our present interest is in the low incident energy phenomena such as fusion and compound nucleus formation, the contribution of the nucleon–nucleon scattering is neglected. A deeper and accurate understanding of the nuclear potential is vital for the accurate fusion analysis. Several recent studies have shown that the outcome of these phenomena depends strongly on the nucleus–nucleus interaction potential one is using. Further, the Coulomb potential alone cannot define the barrier. The nuclear potential plays an equally important role while defining the barrier. This is evident from the fact that lots of efforts are put recently to understand the nuclear part of the potential at an accurate level [2–8]. In this series of recent attempts, the well-known proximity potential has been restructured to remove the gray parts of its first version [8].

This renewed interest in the nuclear potential is also linked with the discoveries of large number of proton as well as neutron-rich nuclei that give unique possibility to test the structural models as well as nuclear potentials at the extremes. The properties of neutron-rich nuclei like ${}^{9-10}{}_{2}\mathrm{He}$ ($N/Z =$ 3.50–4.00), ${}^{8-11}{}_{3}\mathrm{Li}$ ($N/Z = 1.667$–2.667), ${}^{11,14}{}_{4}\mathrm{Be}$ ($N/Z = 1.75, 2.5$), ${}^{14,17,19}{}_{5}\mathrm{B}$ ($N/Z = 1.8, 2.4, 2.8$), ${}^{17,19,22}{}_{6}\mathrm{C}$ ($N/Z = 1.83, 2.167, 2.667$), ${}^{17,22}{}_{7}\mathrm{N}$ ($N/Z = 1.429, 2.143$), ${}^{22,26,28}{}_{8}\mathrm{O}$ ($N/Z = 1.75, 2.25, 2.50$), ${}^{27,29,31}{}_{9}\mathrm{F}$ ($N/Z = 2.0, 2.22, 2.44$), ${}^{29,34}{}_{10}\mathrm{Ne}$ ($N/Z = 1.9, 2.4$), ${}^{20,32,37}{}_{11}\mathrm{Na}$ ($N/Z = 0.818, 1.909, 2.364$), ${}^{40}{}_{12}\mathrm{Mg}$ ($N/Z = 2.333$), ${}^{29,31}{}_{13}\mathrm{Al}$ ($N/Z = 1.231, 1.385$), ${}^{38}{}_{16}\mathrm{S}$ ($N/Z = 1.375$), ${}^{49-51}{}_{18}\mathrm{Ar}$ ($N/Z = 1.722$–1.833), ${}^{60}{}_{20}\mathrm{Ca}$ ($N/Z = 2.0$), ${}^{68-78}{}_{28}\mathrm{Ni}$ ($N/Z = 1.429$–1.786), ${}^{123}{}_{47}\mathrm{Ag}$ ($N/Z = 1.617$), ${}^{123-128}{}_{48}\mathrm{Cd}$ ($N/Z = 1.563$–1.667), ${}^{132}{}_{50}\mathrm{Sn}$ ($N/Z = 1.64$) *etc.* are well understood [9–15]. Lots of efforts are also made to analyse the proton-rich nuclei like ${}^{6}{}_{4}\mathrm{Be}$ ($N/Z = 0.50$), ${}^{10}{}_{7}\mathrm{N}$ ($N/Z = 0.429$), ${}^{12}{}_{8}\mathrm{O}$ ($N/Z = 0.50$), ${}^{17}{}_{9}\mathrm{F}$ ($N/Z = 0.889$), ${}^{17}{}_{10}\mathrm{Ne}$ ($N/Z = 0.70$), ${}^{22}{}_{14}\mathrm{Si}$ ($N/Z = 0.571$), ${}^{31}{}_{18}\mathrm{Ar}$ ($N/Z = 0.722$), ${}^{34}{}_{20}\mathrm{Ca}$ ($N/Z = 0.70$), ${}^{38,39}{}_{22}\mathrm{Ti}$ ($N/Z = 0.0.727, 0.773$), ${}^{45}{}_{26}\mathrm{Fe}$ ($N/Z = 0.731$), ${}^{48,49}{}_{28}\mathrm{Ni}$ ($N/Z = 0.714$–0.75), ${}^{54}{}_{30}\mathrm{Zn}$ ($N/Z = 0.80$) *etc.* [16–24]. A large numbers of these isotopes are also available as primary and secondary nuclear beams.

Although, the above mentioned nuclear potentials have been employed to study the fusion of stable symmetric isotopes, no study is yet available that focuses on comparing these potentials for the collision of β-unstable nuclei. A comparative study employing variety of nuclear potentials may give a model independent view of the role of isotopic dependence in fusion probabilities. It is worth mentioning that most of fusion studies have been performed using either Ca or Ni isotopes [25–36] and recently, we have reported a systematic study of the isotopic dependence of fusion cross-sections within the Skyrme energy density model [37]. Here our present aim is at least two folds:

(i) to compare the different nuclear potentials based on different assumptions and to analyse whether they are similar at the surface or not and *(ii)* to study the isotopic dependence of fusion probabilities using different potentials and to obtain a model independent isotopic dependence. In Section 2, we shall discuss the theoretical framework. Section 3 yields a comparative study of the fusion barriers and cross-sections, whereas our results are summarised in Section 4.

2. Formalism

The total interaction ion–ion potential comprises of nuclear and Coulomb parts:

$$\begin{aligned} V_{\mathrm{T}}(R) &= V_{\mathrm{N}}(R) + V_{\mathrm{C}}(R)\,, \\ &= V_{\mathrm{N}}(R) + \frac{Z_1 Z_2 e^2}{R}\,. \end{aligned} \tag{1}$$

Since fusion happens at a distance larger than the touching configuration of the colliding pair ($> (R_1 + R_2)$, R_i is the radius of either projectile or target), the above form of the Coulomb potential is justified. Once $V_{\mathrm{T}}(R)$ is known, one can extract the barrier height V_{B} and barrier position R_{B} using

$$\left.\frac{dV_{\mathrm{T}}(R)}{dR}\right|_{R=R_{\mathrm{B}}} = 0\,, \quad \text{and} \quad \left.\frac{d^2V_{\mathrm{T}}(R)}{dR^2}\right|_{R=R_{\mathrm{B}}} \leq 0\,. \tag{2}$$

The shape of the barrier gives us possibility to calculate the fusion cross-section accordingly [38]:

$$\sigma_{\mathrm{fus}}(\mathrm{mb}) = \frac{10R_{\mathrm{B}}^2\hbar\omega_0}{2E_{\mathrm{cm}}} \ln\left[1 + \exp 2\pi\left(\frac{E_{\mathrm{cm}} - V_{\mathrm{B}}}{\hbar\omega_0}\right)\right], \tag{3}$$

where E_{cm} is the center-of-mass energy and $\hbar\omega_0$ is the barrier curvature parameter which measures the width of the fusion barrier. Since our present interest is in the incident energies above the Coulomb barrier, Eq. (3) can be replaced by:

$$\sigma_{\mathrm{fus}}(\mathrm{mb}) = 10\pi R_{\mathrm{B}}^2\left[1 - \frac{V_{\mathrm{B}}}{E_{\mathrm{cm}}}\right]. \tag{4}$$

From Eq. (4) it is also evident that the variation in R_{B} has a stronger effect on fusion cross-section compared to barrier height V_{B}. The role of different nuclear potentials $V_{\mathrm{N}}(R)$ can be studied through Eq. (1). We shall use the following potentials in present analysis.

2.1. Skyrme energy density model

One of the most extensively used formalism to study the heavy-ion problems at low as well as intermediate energies is the Skyrme energy density formalism, where energy expectation value is given by [39–41]

$$E = \int H(\vec{r})d\vec{r} \tag{5}$$

leading to the interaction potential

$$V_N\left(R\right) = E\left(R\right) - E\left(\infty\right)\,, \tag{6}$$

i.e. a difference of the expectation values at a distance R and at complete isolation ∞. Following the formalism of Vautherin and Brink [41], the Hamiltonian density is a function of nucleonic density ρ, kinetic energy density τ and spin density $\vec{J}$. Among all parameters, the kinetic energy density τ and spin density $\vec{J}$ are of main interest. Following Refs. [39–41], the kinetic energy density τ can be replaced by:

$$\tau = \tau_{\mathrm{TF}} + \lambda\frac{\left(\vec{\nabla}\rho\right)^2}{\rho} = \frac{3}{5}\left(\frac{3}{2}\pi^2\right)^{2/3}\rho^{5/3} + \lambda\frac{\left(\vec{\nabla}\rho\right)^2}{\rho}\,, \tag{7}$$

where λ is a constant whose value varies between $1/36$ and $9/36$. This approximation, reduces the Hamiltonian dependence to two-parameters, namely, ρ and $\vec{J}$. Therefore, one can write the Hamiltonian as:

$$H\left(\rho,\tau,\vec{J}\right) = H\left(\rho\right) + H\left(\rho,\vec{J}\right)\,. \tag{8}$$

The first part, which is independent of the spin density, is called spin-independent part whereas second part is labelled as spin density dependent part which contains the terms of spin density part [39]. The corresponding potentials are marked as spin-independent potential $V_P(R)$ and spin-dependent potential $V_J(R)$, respectively. In the present study, we use two-parameter Fermi mass density distribution whose parameters are taken from Ref. [38]. A straight-line interpolation is used where data is not available. At present, we do not distinguish between different isotone as remarked in Ref. [39]. It is worth mentioning that we are the first one to extend the spin density part $\vec{J}$ to any even number of valance nucleons outside a closed core. This potential has been shown to explain the fusion data accurately [41]. For the details, the reader is referred to Refs. [39–41]. This potential and calculations are labelled as EDF.

Other potentials, the proximity potential [42], Bass potential [43], Ngô–Ngô potential [44], Christensen and Winther [45], and Denisov [4] are well described in the cited literature and reader is referred to these publications. Note that all the above-mentioned six potentials are well known and have been used successfully in the different problems of nuclear structure and heavy-ion reactions. The common factor in all potentials is that these can be divided as a product of geometrical factor (proportionate to radii) and a universal function which is the same for all colliding nuclei. A study of isotopic dependence of fusion cross-sections with these six potentials will give us possibility to generate a model free and independent conclusion about the isotopic dependence of fusion cross-section in heavy-ion collisions above the Coulomb barrier energies.

3. Results and discussion

As stated in the introduction, the extensively used systems for the fusion analysis are the isotopes of Ca and Ni nuclei, which are also the magic nuclei. Therefore, we also use these systems for our present analysis. Here we start with the symmetric $^{40}\mathrm{Ca}+{}^{40}\mathrm{Ca}$, $^{56}\mathrm{Ni}+{}^{56}\mathrm{Ni}$ and $^{40}\mathrm{Ca}+{}^{56}\mathrm{Ni}$ reactions using the above mentioned different nuclear potentials. The isotopic dependence is investigated by either adding or removing the neutrons gradually from either (or both) the colliding pair and calculating the interaction barrier using different potentials. In the present analysis, the domain of neutron–proton ratio is chosen to be $0.5 \leq N/Z \leq 2.0$.

In figure 1, we display the nuclear, Coulomb and total potentials as a function of the inter-nuclear distance R. We display in (a), (b) and (c) parts of the figure, the potentials using different Skyrme forces and surface correction factors λ. The (a) and (b) parts display the effect of variation in the surface correction λ (with $\lambda = 5/36$ and $\lambda = 9/36$, respectively) whereas part (c) shows the potential with Skyrme force Ska. This comparison gives us possibility to look for the role of different Skyrme forces in isotopic dependence of interaction potentials. It is worth mentioning that the Skyrme force Ska is widely used in recent years for studying the low energy phenomena. Since the present formalism, allows us to analyse each and every term of the Hamiltonian density separately, we display in figure 1(d) the potential due to spin density part of the Hamiltonian only. From parts (a)–(c), it is evident that the well-known isotopic dependence exists for the cases of $\lambda = 5/36$ and $\lambda = 9/36$. The nuclear potential becomes deeper with the addition of neutrons whereas inverse is true with the removal of neutrons. As a result, barrier height increases with the removal of neutrons, and barrier positions are pushed inward. One may say that due to the shifting of barrier positions inwards, the barrier heights get affected accordingly. One

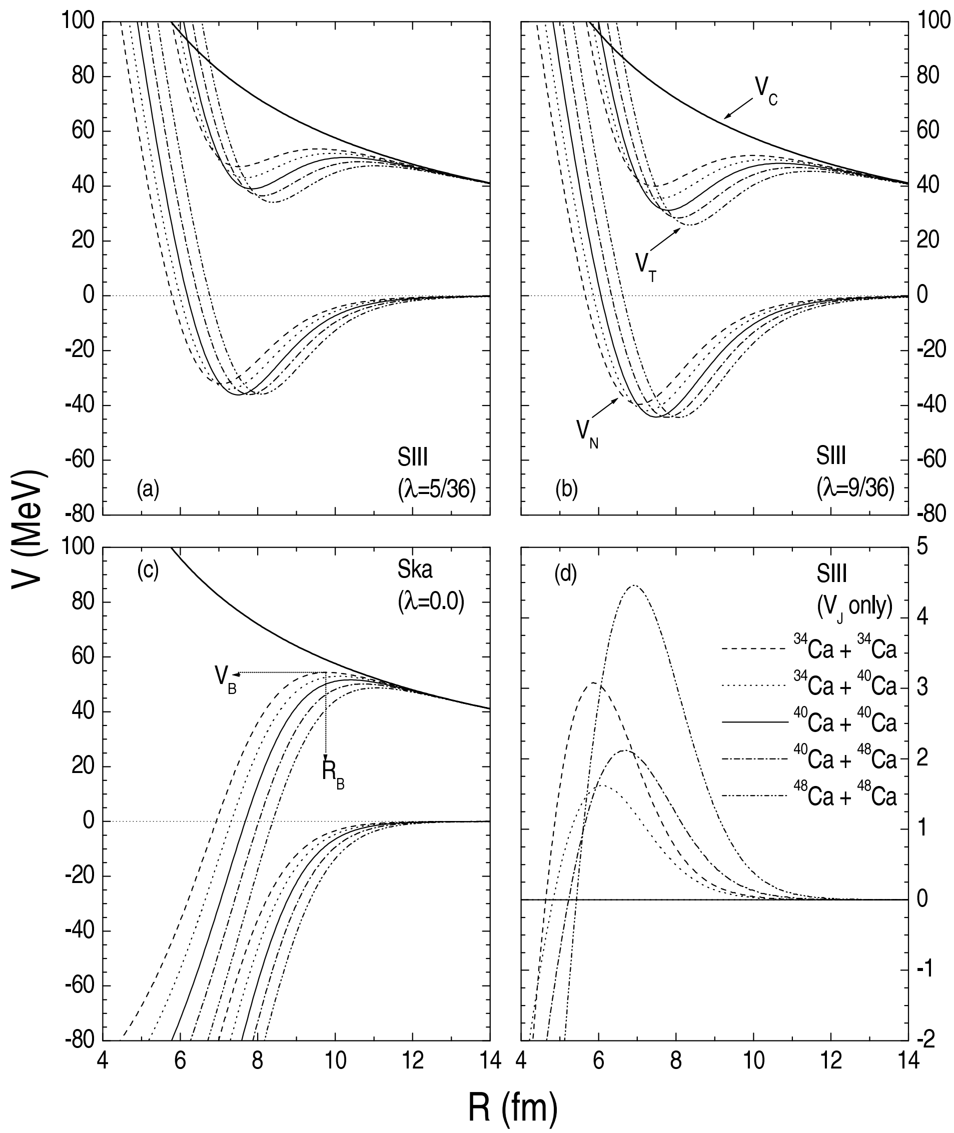

Fig. 1. The nuclear potential $V_{\mathrm{N}}(R)$, Coulomb potential $V_{\mathrm{C}}(R)$ and total interaction potential $V_{\mathrm{T}}(R)$ as a function of the inter-nuclear distance R. The (a), (b), (c) and (d) parts are using Skyrme force SIII, respectively, $\lambda = 5/36$, $\lambda = 9/36$, Ska force as well as spin density potential only. Here neutron-rich as well as neutron-deficient nuclei are considered.

also sees that different values of surface correction coefficient λ do not alter the picture significantly indicating a smaller role for the surface correction coefficient in isotopic dependence studies. From figure 1(c), one notices that the change of force parameters has no bearing on the above drawn conclusions. A well-known feature of the Skyrme force Ska can also be seen where no pocket exists. The part (d) displays the spin dependent potential $V_J(R)$ which reveals a significant isotopic dependence. As has been discussed in our earlier publications [39–45], this contribution depends on the number of valance particles of reacting partners. We see that ^{40}Ca+^{40}Ca, being a double closed shell pair, has zero contribution towards spin density potential V_J whereas contribution increases as one adds or removes neutrons from ^{40}Ca+^{40}Ca core. This is in contrast to the nuclear potential that changes monotonically with the neutron content. From the figure, it is evident that the isotopic spin density dependent potential can have different structural dependence.

For a model independent analysis, we also studied the other nucleus–nucleus potentials due to Blocki *et al.* [42], Bass [43], Ngô and Ngô [44] and Christensen and Winther [45] (not shown here). All these potentials (including the Skyrme energy density potential) show similar isotopic dependence: the barrier heights are enhanced with removal of neutrons whereas barrier positions are shifted outwards with the addition of neutrons. Since fusion occurs at the surface of the colliding pair, it is immaterial to look for the shape of the potentials in the interior parts. Some differences in various potentials, however, were noticed at the surface regions. One should, however, keep in mind that the model ingredients such as the nuclear radii (of projectile and target), nuclear density parameters or even the nature of the forces *etc.* can also have a drastic effect on the interaction potential as well as on the fusion cross-sections. Different potentials use different radii and geometrical factors leading to different mass dependences on the potential.

Before we discuss the isotopic dependence in interaction barriers and fusion cross-sections, using various models, let us compare the outcome of various theoretical fusion barrier positions and heights with empirical values. In Table I, we list the reactions where experimental information about the isotopic dependence is known. For a wider understanding, we also list the reactions involving Ti and Ar isotopes. One can see immediately that our approach with SIII force ($\lambda = 0$) is closest to the experimental data compared to all other theoretical models. In all the approaches, the barrier heights show systematical reduction with the addition of neutrons. The barrier positions also follow a coherent pattern except in couple of cases where experimental data are questionable [27]. A reasonable agreement between experimental values and theoretical models gives faith in various potentials.

TABLE I

Fusion barrier heights V_{B} and position R_{B} using Skyrme Energy Density Model (SEDM) and other theoretical models along with experimental data.

No.	Reaction	Theoretical Models							
		SEDM				Blocki *et al.* [42]		Ngô and Ngô [44]	
		Skyrme Force SIII, $\lambda = 0$		Skyrme Force SIII, $\lambda = 5/36$					
		V_{B}(MeV)	R_{B}(fm)	V_{B}(MeV)	R_{B}(fm)	V_{B}(MeV)	R_{B}(fm)	V_{B}(MeV)	R_{B}(fm)
1.	^{40}Ca+^{40}Ca	54.3	9.73 ± 0.05	50.5	10.28 ± 0.05	57.6	9.18 ± 0.00	57.7	9.21 ± 0.05
2.	^{40}Ca+^{44}Ca	53.4	9.92 ± 0.05	49.7	10.47 ± 0.05	56.6	9.38 ± 0.00	56.7	9.40 ± 0.00
3.	^{40}Ca+^{48}Ca	52.6	10.06 ± 0.05	48.9	10.66 ± 0.05	55.7	9.51 ± 0.05	55.8	9.58 ± 0.00
4.	^{48}Ca+^{48}Ca	51.1	10.40 ± 0.10	47.4	11.00 ± 0.05	54.0	9.89 ± 0.05	54.1	9.94 ± 0.05
5.	^{40}Ca+ ^{58}Ni	73.2	10.07 ± 0.05	68.4	10.62 ± 0.05	77.1	9.67 ± 0.05	77.6	9.61 ± 0.05
6.	^{40}Ca+^{62}Ni	72.3	10.19 ± 0.10	67.7	10.79 ± 0.05	76.1	9.78 ± 0.00	76.6	9.77 ± 0.05
7.	^{40}Ca+ ^{46}Ti	58.8	9.89 ± 0.05	54.8	10.44 ± 0.05	62.2	9.39 ± 0.05	62.4	9.41 ± 0.05
8.	^{40}Ca+ ^{48}Ti	58.4	9.96 ± 0.05	54.3	10.51 ± 0.05	61.7	9.46 ± 0.00	61.9	9.47 ± 0.00
9.	^{40}Ca+ ^{50}Ti	58.0	10.03 ± 0.05	54.0	10.63 ± 0.10	61.2	9.52 ± 0.05	61.4	9.59 ± 0.05
10.	^{48}Ti + ^{58}Ni	78.8	10.25 ± 0.05	73.7	10.85 ± 0.05	82.7	9.89 ± 0.05	83.2	9.87 ± 0.05
11.	^{48}Ti + ^{60}Ni	78.4	10.34 ± 0.05	73.3	10.94 ± 0.05	82.2	10.00 ± 0.05	82.7	9.93 ± 0.00
12.	^{48}Ti + ^{64}Ni	77.5	10.51 ± 0.00	72.5	11.06 ± 0.05	81.2	10.11 ± 0.00	81.7	10.09 ± 0.00
13.	^{46}Ti + ^{64}Ni	78.0	10.39 ± 0.10	73.1	10.99 ± 0.05	81.8	10.04 ± 0.05	82.3	9.97 ± 0.00
14.	^{50}Ti + ^{60}Ni	77.8	10.40 ± 0.05	72.8	11.00 ± 0.05	81.6	10.06 ± 0.00	82.1	10.04 ± 0.05
15.	^{40}Ar+ ^{58}Ni	65.3	10.17 ± 0.10	60.9	10.77 ± 0.05	68.8	9.72 ± 0.05	69.2	9.71 ± 0.00
16.	^{40}Ar+ ^{60}Ni	64.9	10.25 ± 0.05	60.6	10.85 ± 0.05	68.4	9.82 ± 0.05	68.7	9.82 ± 0.05
17.	^{40}Ar+^{62}Ni	64.6	10.34 ± 0.05	60.3	10.89 ± 0.05	68.0	9.88 ± 0.05	68.3	9.87 ± 0.05
18.	^{40}Ar+ ^{64}Ni	64.2	10.37 ± 0.05	60.0	10.97 ± 0.05	67.6	9.93 ± 0.00	67.9	9.92 ± 0.00
19.	^{58}Ni+ ^{58}Ni	99.0	10.26 ± 0.10	92.8	10.91 ± 0.05	103.5	10.10 ± 0.00	104.4	9.96 ± 0.00
20.	^{58}Ni+ ^{64}Ni	97.3	10.56 ± 0.05	91.4	11.16 ± 0.05	101.6	10.31 ± 0.00	102.5	10.17 ± 0.00
21.	^{64}Ni+ ^{64}Ni	95.7	10.82 ± 0.10	90.0	11.37 ± 0.05	99.8	10.48 ± 0.05	100.6	10.43 ± 0.05

TABLE I continued

No.	Reaction	Theoretical Models: Christensen and Winther [45]		Denisov [4]		Bass [43]		Expt.	
		V_B(MeV)	R_B(fm)	V_B(MeV)	R_B(fm)	V_B(MeV)	R_B(fm)	V_B(MeV)	R_B (fm)
1.	$^{40}Ca+^{40}Ca$	54.3	9.91 ± 0.05	55.6	9.51 ± 0.00	54.8	9.72 ± 0.05	52.30 ± 0.5 50.60 ± 2.8 55.60 ± 0.8	8.8 ± 0.5[27] 9.50 ± 0.5[40] 9.10 ± 0.6[40]
2.	$^{40}Ca+^{44}Ca$	53.4	10.11 ± 0.00	54.6	9.68 ± 0.00	53.9	9.91 ± 0.05	51.70 ± 1.2	8.50 ± 0.5[27]
3.	$^{40}Ca+^{48}Ca$	52.6	10.29 ± 0.05	53.8	9.88 ± 0.05	53.0	10.04 ± 0.05	53.2 51.30 ± 1.0	10.08[28] 7.80 ± 0.3[27]
4.	$^{48}Ca+^{48}Ca$	51.0	10.62 ± 0.05	52.1	10.20 ± 0.05	51.4	10.42 ± 0.05	51.7	10.38[28]
5.	$^{40}Ca+\ ^{58}Ni$	72.8	10.40 ± 0.05	74.8	9.94 ± 0.05	73.7	10.09 ± 0.05	73.0 73.36	9.6 ± 0.3[46] 10.20[47]
6.	$^{40}Ca+^{62}Ni$	71.9	10.56 ± 0.05	73.9	10.07 ± 0.05	72.8	10.25 ± 0.05	71.0 72.30	9.5 ± 0.2[46] 10.35[47]
7.	$^{40}Ca+\ ^{46}Ti$	58.7	10.13 ± 0.00	60.1	9.68 ± 0.05	59.2	9.88 ± 0.00	58.03 ± 0.73	9.92 ± 0.08[30]
8.	$^{40}Ca+\ ^{48}Ti$	58.2	10.19 ± 0.00	59.6	9.76 ± 0.05	58.8	9.94 ± 0.05	58.17 ± 0.62	9.97 ± 0.07[30]
9.	$^{40}Ca+\ ^{50}Ti$	57.8	10.31 ± 0.05	59.2	9.88 ± 0.05	58.3	10.06 ± 0.05	58.71 ± 0.61	10.05 ± 0.07[30]
10.	$^{48}Ti+\ ^{58}Ni$	78.1	10.68 ± 0.00	80.3	10.19 ± 0.05	79.1	10.36 ± 0.05	78.8 ± 0.3	9.8 ± 0.3[34]
11.	$^{48}Ti+\ ^{60}Ni$	77.6	10.74 ± 0.05	79.8	10.25 ± 0.00	78.6	10.47 ± 0.05	77.3 ± 0.3	10.0 ± 0.3[34]
12.	$^{48}Ti+\ ^{64}Ni$	76.7	10.90 ± 0.00	78.9	10.37 ± 0.05	77.7	10.58 ± 0.05	76.7 ± 0.3	10.2 ± 0.3[34]
13.	$^{46}Ti+\ ^{64}Ni$	77.3	10.83 ± 0.05	79.5	10.30 ± 0.05	78.3	10.51 ± 0.05	76.9 ± 0.1	9.7 ± 0.2[35]
14.	$^{50}Ti+\ ^{60}Ni$	77.1	10.85 ± 0.05	79.2	10.33 ± 0.05	78.1	10.53 ± 0.00	77.1 ± 0.1	9.8 ± 0.2[35]
15.	$^{40}Ar+\ ^{58}Ni$	65.1	10.50 ± 0.05	66.7	10.03 ± 0.05	65.7	10.24 ± 0.05	65.3 ± 0.5[32]	
16.	$^{40}Ar+\ ^{60}Ni$	64.7	10.56 ± 0.00	66.2	10.09 ± 0.10	65.3	10.30 ± 0.00	65.5 ± 0.6[32]	
17.	$^{40}Ar+^{62}Ni$	64.3	10.61 ± 0.05	65.9	10.15 ± 0.05	64.9	10.35 ± 0.00	65.1 ± 0.6[32]	
18.	$^{40}Ar+\ ^{64}Ni$	63.9	10.67 ± 0.05	65.5	10.26 ± 0.05	64.6	10.45 ± 0.05	63.9 ± 0.5[32]	
19.	$^{58}Ni+\ ^{58}Ni$	97.7	10.89 ± 0.00	100.7	10.32 ± 0.00	99.3	10.51 ± 0.00	97.90	8.30[33]
20.	$^{58}Ni+\ ^{64}Ni$	96.0	11.11 ± 0.00	99.0	10.51 ± 0.05	97.5	10.72 ± 0.05	96.0	8.20[33]
21.	$^{64}Ni+\ ^{64}Ni$	94.4	11.28 ± 0.00	97.3	10.74 ± 0.00	95.8	10.94 ± 0.05	93.50	8.60[33]

In figure 2, we display the fusion cross-sections for the reactions involving Ca and Ni isotopes using all six potentials. In the case of SIII, we also display the results with $\lambda = 0$ and $\lambda = 5/36$. Here a sharp cut-off $\left(\sigma_{\mathrm{fus}}(\mathrm{mb}) = 10\pi R_{\mathrm{B}}^2[1 - V_{\mathrm{B}}/E_{\mathrm{cm}}]\right)$ model is used for the fusion cross-sections. One observes that some models are able to explain the data very well whereas others either are at the limits or fail to explain the data.

As stated in the introduction, our present interest is to understand the isotopic dependence in fusion probabilities. Therefore, we define the reduced fusion barrier heights, positions as well as cross-sections:

$$\Delta R_{\mathrm{B}}\,(\%) \;=\; \frac{R_{\mathrm{B}} - R_{\mathrm{B}}^0}{R_{\mathrm{B}}^0}\,100\,, \tag{9}$$

$$\Delta V_{\mathrm{B}}\,(\%) \;=\; \frac{V_{\mathrm{B}} - V_{\mathrm{B}}^0}{V_{\mathrm{B}}^0}\,100\,, \tag{10}$$

and

$$\Delta\sigma_{\mathrm{fus}}\,(\%) = \frac{\sigma_{\mathrm{fus}}\left(E_{\mathrm{cm}}^0\right) - \sigma_{\mathrm{fus}}^0\left(E_{\mathrm{cm}}^0\right)}{\sigma_{\mathrm{fus}}^0\left(E_{\mathrm{cm}}^0\right)}\,100\,. \tag{11}$$

Here V_{B}^0, R_{B}^0 and E_{cm}^0 are, respectively, the barrier height, position and center-of-mass energy for $N = Z$ colliding pair. The main advantage of these reduced quantities is that it gives a direct variation over $N = Z$ counter parts. In all the cases where data for $N = Z$ colliding pair is not available, a straight-line interpolation is used. In figure 3, we display $\Delta R_{\mathrm{B}}(\%)$ for all above six potentials. The corresponding barrier heights are displayed in figure 4. Interestingly, all different potentials show a unique isotopic dependence in $\Delta R_{\mathrm{B}}(\%)$ and $\Delta V_{\mathrm{B}}(\%)$. The barrier positions increase with the addition of neutrons that reduce the barrier heights. Inverse happens for the case of neutron-deficient nuclei. One also notices a linear relationship between $\Delta R_{\mathrm{B}}(\%)/\Delta V_{\mathrm{B}}(\%)$ with N/Z ratio for $N/Z > 1$ and $N/Z < 1$, separately ($= \alpha((N/Z)-1)$; α being a constant that depends on the potential one is using). The point to note here is that the dependence of the $\Delta R_{\mathrm{B}}(\%)$ and $\Delta V_{\mathrm{B}}(\%)$ for neutron-rich ($N/Z > 1$) and neutron-deficient ($N/Z < 1$) regions is different. This happens because the variation in V_{N} with neutrons differs for proton-rich and deficient cases. The different isotopic dependences for neutron-rich and deficient cases can also be parameterized by a single second order non-linear form $= \beta((N/Z)-1)+\gamma((N/Z)-1)^2$. Interestingly, one sees from figures 3 and 4 that the scattering around the mean values is very small for all the cases expect for the Skyrme force SIII. This happens because of the fact that Skyrme force includes also the spin density potential that varies with the valance particles of the colliding pair. This variation results in the above noticed scattering around the mean values. In all the

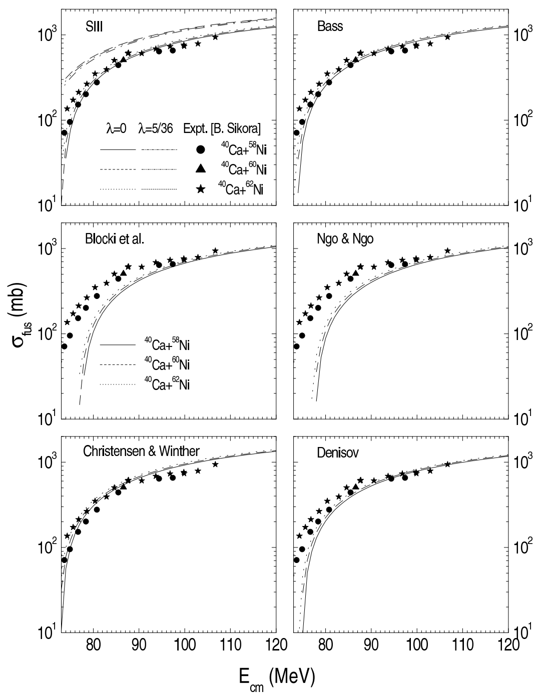

Fig. 2. The fusion cross-sections $\sigma_{\rm fus}$(mb) as a function of centre-of-mass energy $E_{\rm cm}$ for the reactions ^{40}Ca + ^{58}Ni, ^{40}Ca + ^{6}0Ni, ^{40}Ca + ^{62}Ni. We display theoretical results using Skyrme force SIII and proximity potential, as well as parameterized potentials due to Bass, Ngô and Ngô, Christensen and Winther, and Denisov. The experimental data is taken from Sikora *et al.* [46].

cases, our fits are quite close to the calculated ones. One also sees that the slopes of $\Delta R_{\rm B}(\%)/\Delta V_{\rm B}(\%)$ in all different models are very close to each other. The isotopic dependence in all theoretical models for $\Delta R_{\rm B}(\%)$ falls within a limit of 24.25 ± 3.25 for $N/Z<1$, 18.00 ± 1.5 for $N/Z>1$. Whereas for $\Delta V_{\rm B}(\%)$, it is -22.20 ± 1.80 for $N/Z<1$, -15.00 ± 0.50 for $N/Z>1$. The coefficient β and γ for unified formula are within a range of 22.00 ± 3.00 and -4.75 ± 1.75 for $\Delta R_{\rm B}(\%)$ and -18.75 ± 1.25 and 6.80 ± 1.70 for $\Delta V_{\rm B}(\%)$, respectively (see Tables IIa and IIb). In other words, different theoretical models based on quite varying physical picture converge into similar results for isotopic dependence of fusion probabilities. Experiments are called for to verify these our predictions. This is not surprising since every potential can be decomposed into a geometrical factor and universal function. Except for the case of proximity potential and Denisov potential, all other potentials do not have isotopic dependence in the universal function. Therefore, larger part of isotopic dependence is expected from the geometrical parts. This point will be further discussed in the following paragraphs.

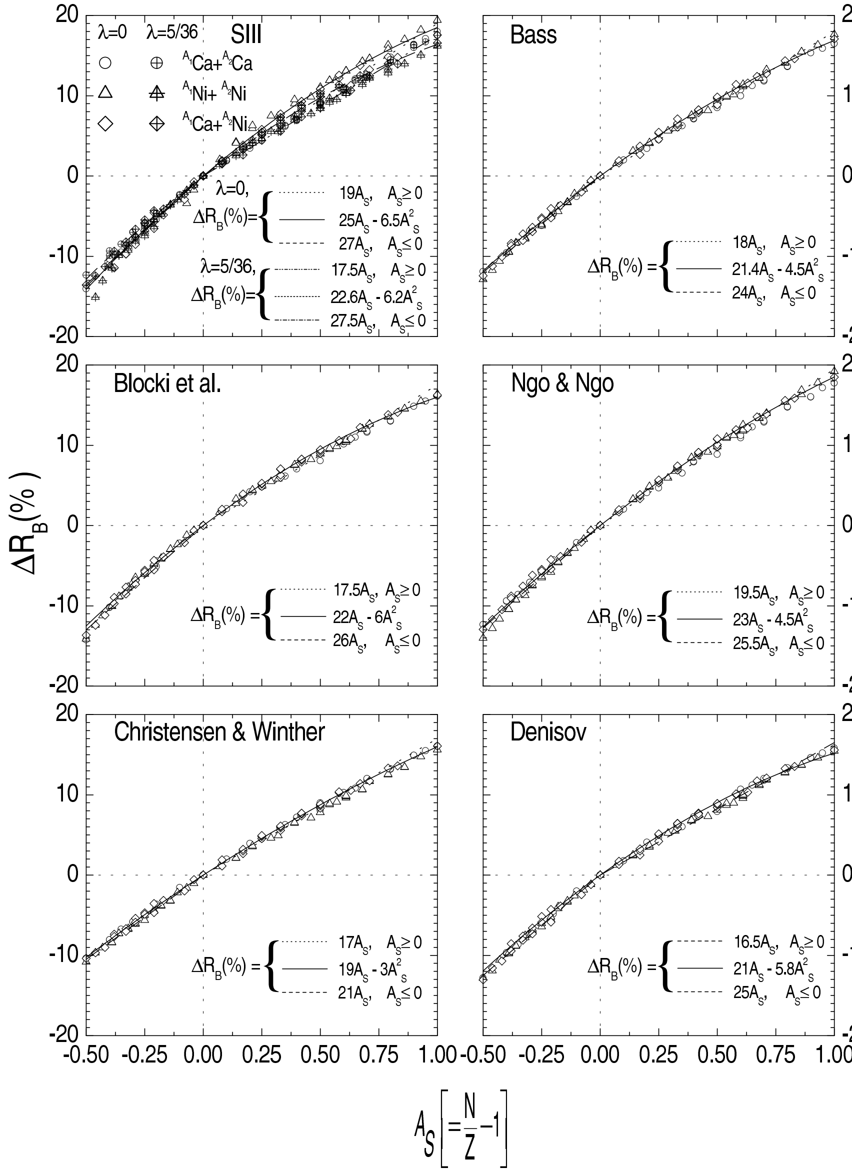

Fig. 3. The $\Delta R_{\rm B}(\%)$ as a function of A_S. We here display the results for 127 reactions using the isotopes Ca and Ni. The dotted line is for $N/Z > 1$ whereas the dashed line is for $N/Z < 1$. The solid line is a fit over full range of neutron as well as proton content.

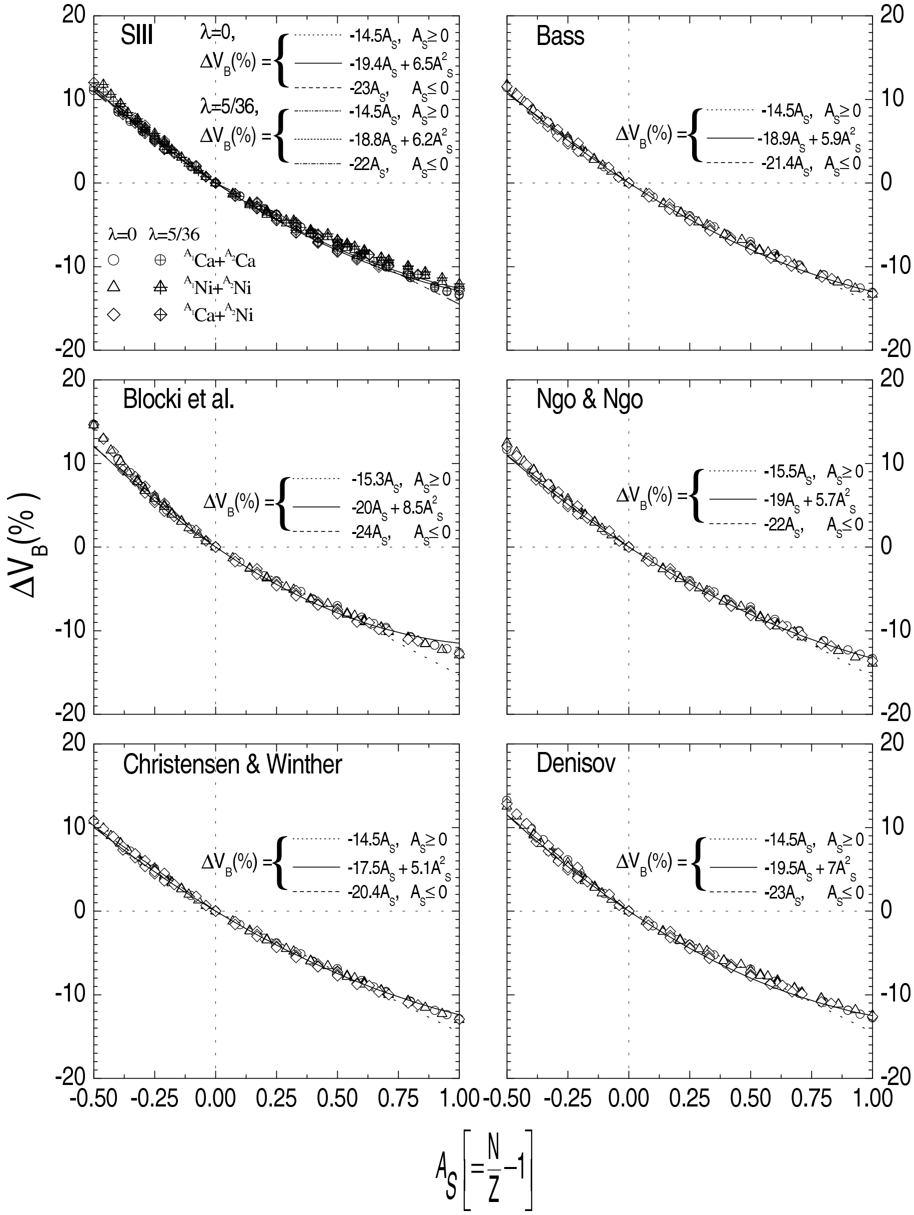

Fig. 4. Same as figure 3, but for $\Delta V_{\mathrm{B}}(\%)$.

TABLE IIa

The coefficient (α) appearing in the parametrization of isotopic variations in fusion barrier heights $\Delta V_{\mathrm{B}}(\%)$ and positions $\Delta R_{\mathrm{B}}(\%)$.

	SEDM Skyrme Force SIII		Blocki *et al.* [42]	Ngô & Ngô [44]	Christensen & Winther [45]	Denisov [4]	Bass [43]
	$\lambda=0$	$\lambda=5/36$					
	α	α	α	α	α	α	α
$\Delta R_{\mathrm{B}}\left(\left[\frac{N}{Z}-1\right]\leq 0\right)$	27.0	27.5	26.0	25.5	21.0	25.0	24.0
$\Delta R_{\mathrm{B}}\left(\left[\frac{N}{Z}-1\right]\geq 0\right)$	19.0	17.5	17.5	19.5	17.0	16.5	18.0
$\Delta V_{\mathrm{B}}\left(\left[\frac{N}{Z}-1\right]\leq 0\right)$	−23.0	−22.0	−24.0	−22.0	−20.4	−23.0	−21.4
$\Delta V_{\mathrm{B}}\left(\left[\frac{N}{Z}-1\right]\geq 0\right)$	−14.5	−14.5	−15.3	−15.5	−14.5	−14.5	−14.5

TABLE IIb

Various coefficients appearing in the parametrization of isotopic variations in fusion barrier heights $\Delta V_{\mathrm{B}}(\%)$ and positions $\Delta R_{\mathrm{B}}(\%)$, Nuclear and Coulomb potential at barrier, $\Delta V_{\mathrm{N}}(\%)$ and $\Delta V_{\mathrm{C}}(\%)$, respectively.

	SEDM Skyrme Force SIII				Blocki *et al.* [42]		Ngô & Ngô [44]		Christensen & Winther [45]		Denisov [4]		Bass [43]	
	$\lambda=0$		$\lambda=5/36$											
	β	γ	β	γ	β	γ	β	γ	β	γ	β	γ	β	γ
$\Delta R_{\mathrm{B}}\left(-0.5\leq\left[\frac{N}{Z}-1\right]\leq 1\right)$	25	−6.5	22.6	−6.2	22.0	−6.0	23.0	−4.5	19.0	−3.0	21.0	−5.8	21.4	−4.5
$\Delta V_{\mathrm{B}}\left(-0.5\leq\left[\frac{N}{Z}-1\right]\leq 1\right)$	−19.4	6.5	−18.8	6.2	−20.0	8.5	−19.0	5.7	−17.5	5.1	−19.5	7.0	−18.9	5.9
$\Delta V_{\mathrm{N}}\left(-0.5\leq\left[\frac{N}{Z}-1\right]\leq 1\right)$	-	-	-	-	−46.6	22	-	-	-	-	-	-	-	-
$\Delta V_{\mathrm{C}}\left(-0.5\leq\left[\frac{N}{Z}-1\right]\leq 1\right)$	-	-	-	-	−23.1	9.8	-	-	-	-	-	-	-	-

Let us now further examine the above second order non-linear behaviour of $\Delta R_{\mathrm{B}}(\%)$) and $\Delta V_{\mathrm{B}}(\%)$. As stated above, all theoretical potentials can be written in terms of a product comprising of geometrical factor ($\overline{R}$); being reduced radius and a universal function ϕ. Since ϕ is a universal function, therefore, the above isotopic dependence could results from the ($\overline{R}$) variation that happens due to the mass variation with addition or removable of neutrons. Therefore, we parameterized $\Delta\overline{R}(\%)$ as a function of $A_S=((N/Z)-1)$ ratio (radius taken from Ref. [44]) and noted a monotonic variation with the change in the neutron contents which is given by a second order non-linear fit with $\Delta\overline{R}(\%)=\beta A_S+\gamma A_S^2$; with $\beta=19.60$, $\gamma=-2.80$ which is quite close to what has been noticed in the case of $\Delta R_{\mathrm{B}}(\%)$ variation, respectively. In other words, it seems that major part of $\Delta R_{\mathrm{B}}(\%)$ variation emerges from the geometrical factors of the potentials rather than from the structural effects. Let us also examine the variation in the nuclear part of the potential with neutron content. In figure 5, we display the universal function ϕ as well as complete nuclear part using proximity potential of Blocki *et al.* [42]. As the name suggests, ϕ is indeed universal throughout the neutron variation and has no structural effects for the isotopic dependence. On the other hand, nuclear potential (that also includes the geometrical factor) has a monotonic isotopic dependence. Naturally, nuclear potential is different for different colliding series like Ca+Ca, Ca+Ni and Ni+Ni; being deepest for Ni+Ni and shallow for Ca+Ca. Interestingly, nuclear part increases with the removal of neutrons. This is in contradiction to the couple of earlier calculations where it was concluded that the nuclear part of the potential is more attractive with the addition of neutrons leading to reduced barrier [46]. Note that for the cases of neutron-deficient nuclei, not only the nuclear potential becomes more attractive, but at the same time, the Coulomb forces become stronger, therefore, their mutual dominance decides

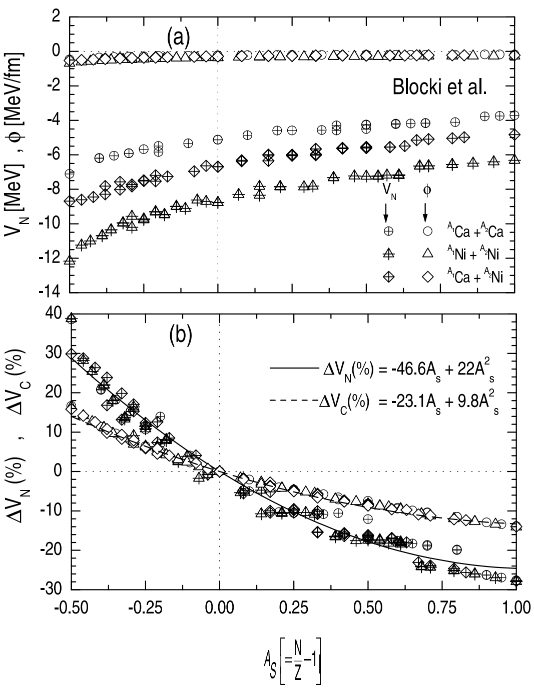

Fig. 5. (a) The universal as well as absolute nuclear potential as a function of A_S for ^{A_1}Ca + ^{A_2}Ca, ^{A_1}Ni + ^{A_2}Ni and ^{A_1}Ca + ^{A_2}Ni within proximity potential. (b) $\Delta V_{\mathrm{N}}(\%)$ and $\Delta V_{\mathrm{C}}(\%)$ variation within proximity potential.

about the barrier height. However, the increase in the Coulomb potential (due to the removal of neutrons) is much more than the corresponding nuclear potential, therefore, enhancing the fusion barriers when neutrons are removed.

Let us now examine how fusion cross-section varies with the neutron content. Since, the fusion cross-section depends also on the incident energies, we shall discuss these systematics in terms of the reduced incident energies $E^0_{\rm cm}$ that correspond to the $N = Z$ symmetric pair. In figure 6, we display the variation in the fusion probabilities with the change in the isotopic content. For an illustrative example, we took $E^0_{\rm cm} = 1.25V^0_{\rm B}$. Interestingly, a linear isotopic dependence occurs for the fusion probability in all the cases. This is important, since in spite of the different dependences of $\Delta R_{\rm B}(\%)$ and $\Delta V_{\rm B}(\%)$ for $N/Z > 1$ and $N/Z < 1$ region, a linear variation occurs for the fusion probabilities. All fusion variation $\Delta\sigma_{\rm fus}(\%)$ lie within 112.50 ± 6.50 justifying the universality in these theoretical studies. The energy dependence of the isotopic slope in different theoretical models was also examined in similar manner. From the analysis, we concluded that: *(i)* the impact of isotopic dependence in the fusion cross-sections is drastic for the near Coulomb barrier energies, which decreases with the increase in the incident energy. At very high incident energies, the isotopic dependence reduces to insignificant level. This observation is independent of the theoretical models and is also in agreement with other findings. It is worth mentioning that the maximal effect of isotopic dependence is found at sub-barrier region. *(ii)* Since, all theoretical models yield similar dependence, one may predict universal values to be $948.00 \pm 42, 645.25 \pm 29.25, 493.85 \pm 22.85, 342.40 \pm 16.40, 281.85 \pm 13.85, 221.30 \pm 11.30, 185.05 \pm 9.65, 160.85 \pm 8.55, 112.50{\pm}6.50, 100.25{\pm}6.05, 88.10{\pm}5.50, 82.45{\pm}5.25$, and $76.00{\pm}5.00$ for $E^0_{\rm cm} = 1.02V^0_{\rm B}$, $1.03V^0_{\rm B}$, $1.04V^0_{\rm B}$, $1.06V^0_{\rm B}$, $1.075V^0_{\rm B}$, $1.10V^0_{\rm B}$, $1.125V^0_{\rm B}$, $1.15V^0_{\rm B}$, $1.25V^0_{\rm B}$, $1.30V^0_{\rm B}$, $1.375V^0_{\rm B}$, $1.425V^0_{\rm B}$, and $1.50V^0_{\rm B}$. It is further interesting to note that all theoretical models converge to $\pm 14.01\%$. The experiments are called for to verify these predictions.

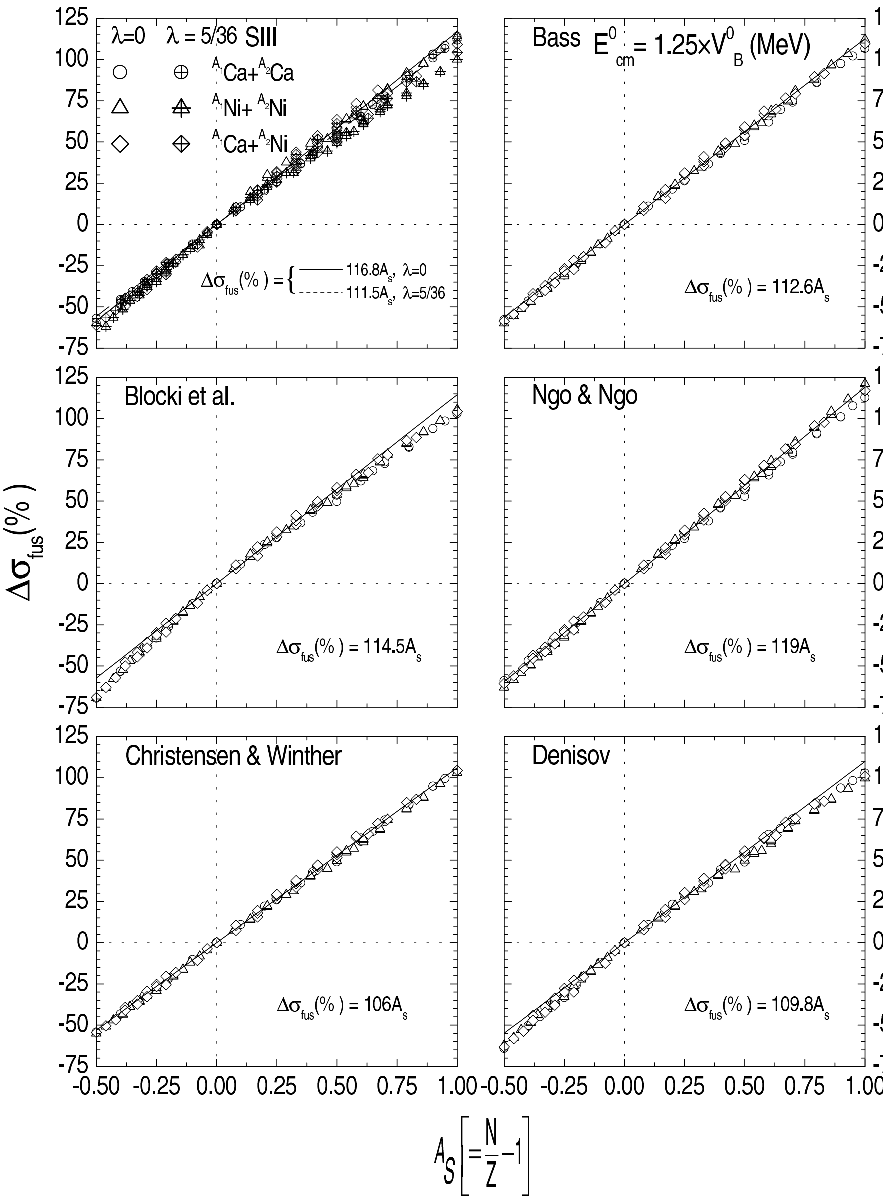

Fig. 6. Same as figure 3, but for $\Delta\sigma_{\rm fus}(\%)$ as a function of A_S.

4. Summary

In this paper, we presented a unified description of isotopic dependence of fusion barriers and cross-sections. This was done by analysing three series of colliding nuclei namely, Ca+Ca, Ca+Ni and Ni+Ni, which have been studied extensively for the study of fusion dynamics. The isotopic dependence was examined by either adding neutrons gradually to either of nuclei (neutron-rich nuclei $N/Z > 1$) or by removing neutrons from colliding nuclei (neutron-deficient nuclei $N/Z < 1$). For a model independent analysis, we employed Skyrme energy density model extended to spin-unsaturated nuclei with two typical forces SIII and Ska, the proximity potential that divides the potential into a universal function and geometrical factor; as well as parameterized potentials due to Ngô and Ngô, Christensen and Winther, Denisov and Bass. Our findings reveal that a second order non-linear isotopic dependence exists for the variation in normalised fusion barrier positions and barrier heights, independent of the theoretical approach. This dependence can be explained in terms of geometrical factors. As a consequence, a linear dependence exists for the isotopic variation in fusion probabilities. The fusion probabilities are maximal near the fusion barrier energies that diminish to insignificant level at higher incident energies. Summarising, a model independent and unified isotopic dependence of normalised fusion probability is given in terms of a second order non-linear behaviour.

This work is supported by the Department of Atomic Energy, Board of Research in Nuclear Sciences Grant No. 2005/37/32/BNRS.

REFERENCES

[1] J. Aichelin, *Phys. Rep.* **202**, 233 (1991); Ch. Hartnack *et al., Eur. Phys. J.* **A1**, 151 (1998).

[2] Basudeb Sahu *et al., Phys. Rev.* **C57**, 1853 (1998).

[3] R.K. Puri, M.K. Sharma, R.K. Gupta, *Eur. Phys. J.* **A3**, 277 (1998).

[4] V.Yu. Denisov, *Phys. Lett.* **B526**, 315 (2002).

[5] A. Dobrowolski, K. Pomorski, J. Bartel, *Nucl. Phys.* **A729**, 713 (2003).

[6] D.M. Brink, C.V. Sukumar, *Nucl. Phys.* **A697**, 689 (2002).

[7] M. Ismail, M.M. Osman, F. Salah, *Phys. Lett.* **B378**, 40 (1996).

[8] W.D. Mayers, W.J. Swiatecki, *Phys. Rev.* **C62**, 044610 (2000).

[9] S.M. Lukyanov *et al., J. Phys. G: Nucl. Part. Phys.* **28**, L41 (2002).

[10] A. Leistenschneider *et al., Phys. Rev. Lett.* **86**, 5442 (2001).

[11] J.F. Liang *et al., Nucl. Phys.* **A746**, 103 (2004).

[12] S. Aoyama, K. Kato, K. Ikeda, *Phys. Rev.* **C55**, 2379 (1997).

[13] T. Suzuki *et al., Phys. Rev. Lett.* **75**, 3241 (1995).

[14] X.R. Zhou *et al., Nucl. Phys.* **A723**, 375 (2003).

[15] L. Weissman *et al., Phys. Rev.* **C67**, 054314 (2003); H. Scheit *et al., Phys. Rev.* **C63**, 014604 (2001).

[16] T. Ishii *et al., Eur. Phys. J.* **A13**, 15 (2002).

[17] E. Caurier *et al., Phys. Rev.* **C58**, 2033 (1998).

[18] H. Mach *et al., Phys. Rev.* **C34**, 1117 (1986).

[19] O.N. Malyshev *et al., Eur. Phys. J.* **A8**, 295 (2000).

[20] J. Giovinazzo *et al., Eur. Phys. J.* **A10**, 73 (2001).

[21] B.J. Cole, *Phys. Rev.* **C54**, 1240 (1996).

[22] A. Lépine-Szily *et al., Phys. Rev.* **C65**, 054318 (2002).

[23] B. Blank *et al., Phys. Rev.* **C54**, 572 (1996); *Phys. Rev. Lett.* **77**, 2893 (1996).

[24] O.V. Bochkorev *et al., Sov. J. Nucl. Phys.* **55**, 955 (1992); D.F. Geesaman *et al., Phys. Rev.* **C15**, 1835 (1977).

[25] T. Udagawa, *Phys. Rev.* **C32**, 124 (1985).

[26] V. Borrel *et al., Nucl. Phys.* **A473**, 331 (1987).

[27] H.A. Aljuwair *et al., Phys. Rev.* **C30**, 1223 (1984).

[28] M. Trotta *et al., Phys. Rev.* **C65**, 011601(R) (2001).

[29] V.I. Zagrebaev, *Phys. Rev.* **C67**, 061601(R) (2003).

[30] A.A. Sanzogni *et al., Phys. Rev.* **C57**, 722 (1998).

[31] C.L. Jiang *et al., Phys. Rev. Lett.* **89**, 052701 (2002).

[32] U. Jahnke *et al., Phys. Rev. Lett.* **48**, 17 (1982).

[33] M. Beckerman, *et al., Phys. Rev.* **C25**, 837 (1982).

[34] A.M. Vinodkumar *et al., Phys. Rev.* **C53**, 803 (1996).

[35] N.V.S.V. Prasad *et al., Nucl. Phys.* **A603**, 176 (1996).

[36] C.P. Silva *et al., Phys. Rev.* **C55**, 3155 (1997).

[37] R.K. Puri, Narinder Dhiman, *Eur. Phys. J.* **A23**, 429 (2005).

[38] C.Y. Wong, *Phys. Lett.* **32B**, 567 (1970); *Phys. Lett.* **42B**, 186 (1972); *Phys. Rev. Lett.* **31**, 766 (1973).

[39] R.K. Puri, P. Chattopadhyay, R.K. Gupta, *Phys. Rev.* **C43**, 315 (1991).

[40] R.K. Puri, R.K. Gupta, *Phys. Rev.* **C45**, 1837 (1992).

[41] D. Vautherin, D.M. Brink, *Phys. Rev.* **C5**, 626 (1972).

[42] J. Blocki *et al., Ann. Phys. (NY)* **105**, 427 (1977).

[43] R. Bass, *Phys. Rev. Lett.* **39**, 265 (1977); *Nucl. Phys.* **A231**, 45 (1974).

[44] H. Ngô, C. Ngô, *Nucl. Phys.* **A348**, 140 (1980).

[45] P.R. Christensen, A. Winther, *Phys. Lett.* **B65**, 19 (1976).

[46] B. Sikora *et al., Phys. Rev.* **C20**, 2219 (1979).

[47] L.C. Vaz, J.M. Alexander, G.R. Satchler, *Phys. Rep.* **69**, 373 (1981).